SIAM J. APPL. MATH.
Vol. 62, No. 2, pp. 385–406
© 2001 Society for Industrial and Applied Mathematics

SINGULARITIES IN HELE–SHAW FLOWS DRIVEN BY A MULTIPOLE*

QING NIE† AND FEI-RAN TIAN‡

Abstract. We study, analytically and numerically, singularity formation in an interface flow driven by a multipole for a two-dimensional Hele–Shaw cell with surface tension. Our analysis proves that singularity formation is inevitable in the case of a dipole. For a multipole of a higher order, we show that the solution does not tend to any stationary solution as time goes to infinity if its initial center of mass is not at the multipole; it is therefore very likely that this solution will develop finite time singularities. Our extensive numerical studies suggest that a solution develops finite time singularities via the interface reaching the multipole while forming a corner at the tip of the finger that touches the multipole. In addition, it is observed that the interface approaches the multipole from directions which can be predicted beforehand. We also estimate as a function of time the distance between the finger tip and multipole, and the results are in excellent agreement with numerical computations.

Key words. Hele–Shaw, interface, singularity

AMS subject classifications. 76S05, 76D, 76M

PII. S0036139900374192

1. Introduction.

Flow in a porous medium is a challenging scientific problem of great technological importance. For the case of two immiscible fluids, it is well known that the interface will be unstable when the less viscous fluid drives the more viscous fluid [2]. This instability is responsible for water flooding of oil wells and is of great interest to oil reservoir engineering and many other applications.

In order to study this instability, experiments have been performed in a Hele–Shaw cell: a channel formed by two closely spaced parallel glass plates. For simplicity, we consider two fluids within the cell: one with high viscosity and the other with low viscosity (regarded as inviscid). The viscous fluid is governed by three-dimensional Stokes equations. For a gap that is sufficiently small compared with the radial dimension, the three-dimensional Stokes equations may be averaged across the gap to give Darcy's law [2]. This provides a model of two-dimensional flow through a porous medium. The pressure jump across the interface which separates these two fluids is balanced by the surface tension. By the use of sinks and sources in the viscous fluid, we may model the behavior of flows in porous media in and around oil wells. The fluid velocity potential has logarithmic singularities at the sinks and sources. When these sinks and sources have large intensity and lie close to each other, the logarithmic singularities become multipole singularities [4].

When the flow is driven by a sink, generic Hele–Shaw solutions break down before all the fluid is sucked out. In the absence of surface tension, all solutions except the circular ones develop singularities, which include formation of cusps at the interface, topological changes, and the interface's reaching the sink [7, 16]. In the presence of surface tension, analytic, numerical, and experimental evidence show that generic

*Received by the editors June 19, 2000; accepted for publication (in revised form) April 10, 2001; published electronically October 18, 2001. The research of this author was partially supported by National Science Foundation grant DMS 0074414.
http://www.siam.org/journals/siap/62-2/37419.html
†Department of Mathematics, University of California, Irvine, CA 92697 (qnie@math.uci.edu).
‡Department of Mathematics, The Ohio State University, 231 West 18th Avenue, Columbus, OH 43210 (tian@math.ohio-state.edu).

solutions form singularities via the interface's reaching the sink before all the fluid is gone [8, 10, 3, 11, 15].

In this paper, we study Hele–Shaw flows driven by a multipole. Because a multipole produces no net mass change in the fluid, intuitively it may be possible that a flow solution can exist for all time. However, in the absence of surface tension it is found that all flow solutions must become singular in finite times [4].

Surface tension is therefore included to mimic realistic physical situations and to regularize the singularities mathematically. For some solutions, singularity formation is immediately prevented. Indeed, there exist stationary solutions. These time-independent solutions were constructed by Entov, Etingof, and Kleinbock [4]. The solutions possess the following important properties:

1. The order of the multipole is greater than 1.
2. The center of the fluid domain is at the multipole.
3. The surface tension is sufficiently large.

The purpose of this paper is to study the time-dependent solution driven by a multipole in the presence of surface tension. We would like to understand whether and how the solution will form singularities in a finite time.

Since stationary solutions can be considered as equilibrium solutions, it is likely that some time-dependent solutions satisfying the above properties approach them as time goes to the infinity. Indeed, Kelley and Hinch's computations suggest that this is true in the case of a quadrupole [9]. In this paper, we will also present numerical evidence to confirm this large time behavior not only in the case of a quadrupole but also in the case of a multipole of order 3.

It is also plausible that violation of any of the above three properties will lead to finite time singularities. The main part of this paper presents strong analytical and computational evidence to support this observation.

The organization of this paper is as follows. In section 2, rigorous analysis is carried out mainly for the nonzero surface tension case. We prove that singularity formation is inevitable in the case of a dipole. For a multipole of a higher order, we show that the solution does not approach any stationary solution as $t \to +\infty$ if its initial center of mass is not at the multipole; it is therefore very likely that the solution will develop finite time singularities for this case. In addition, new exact solutions for zero surface tension are presented. In section 3, the numerical method for computing this system is described. In section 4, we discuss the numerical results for nonzero surface tension with various initial interfaces. These include those initial interfaces presented in section 2 for zero surface tension. We point out the main phenomena: the development of long fingers on the interface, the movement of the fingers towards the multipole from predictable directions, and the formation of corners at the finger tips as they reach the sink. Finally, we derive an asymptotic formula for the distance between the finger tip and multipole as they get close to each other.

2. Breakdown of solutions. The dynamics of a two-dimensional Hele–Shaw flow driven by a multipole are determined as follows [2, 12, 15]. First, one solves a Dirichlet problem for the Laplace equation in a domain with a given singularity at a fixed interior point, say the origin:

$$\phi_{xx} + \phi_{yy} = 0 \qquad \text{in } \Omega(t)\backslash(0,0), \tag{1}$$

$$\phi = \tau\kappa \qquad \text{on } \partial\Omega(t), \tag{2}$$

$$\phi \sim -M\mathrm{Re}\left\{\frac{1}{(x+\mathrm{i}y)^p}\right\} + O(1) \qquad \text{as } (x,y) \longrightarrow (0,0), \tag{3}$$

where $\Omega(t)$ is a simply connected domain with a smooth boundary $\partial\Omega(t)$, κ is the curvature with the requirement that it is negative when $\Omega(t)$ is convex, τ is the surface tension parameter, and the positive integer p is the order of the multipole. The solution uniquely exists and depends smoothly on time. One then uses the solution $\phi(x, y, t)$ to determine the motion of the boundary $\partial\Omega(t)$ by

$$V_n = \frac{\partial \phi}{\partial \vec{n}} \quad \text{on } \partial\Omega(t), \tag{4}$$

where $\vec{n}$ is the outward normal vector to $\partial\Omega(t)$, and V_n is the normal component of the velocity of $\partial\Omega(t)$.

Physically, the viscous fluid occupies the domain $\Omega(t)$, and the inviscid one its complement. The function ϕ is the viscous fluid velocity potential identified with the fluid-pressure field (Darcy's law). Equation (1) follows from the facts that ϕ is the velocity potential and that the viscous fluid is incompressible. The pressure in the nonviscous fluid is taken to be constant, say zero. Relation (2), which is the Laplace–Young relation, thus represents the jump of pressure across the interface $\partial\Omega(t)$. Equation (3) indicates that the origin is a multipole of order p. Finally, (4) expresses the concept that $\partial\Omega(t)$ is a material curve.

A multipole can be viewed as the limiting case of a combination of sinks and sources. Namely, a simple calculation shows that

$$-M\mathrm{Re}\left\{\frac{1}{(x+\mathrm{i}y)^p}\right\} = \lim_{\epsilon\to 0}\sum_{k=0}^{2p-1}(-1)^k\frac{M}{2\epsilon^p}\log|x+iy-\epsilon e^{\frac{ik\pi}{p}}|. \tag{5}$$

Each term in the sum is a sink or source of strength $(-1)^k\frac{M}{2\epsilon^p}$ located at the point $z = \epsilon e^{ik\pi/p}$; odd k corresponds to a sink and even k to a source [4]. This viewpoint will later be used to determine the preferred directions in the motion of the interface.

Hele–Shaw flows driven by sinks and sources have been extensively studied. One of the ideas is to capture the motion of the interface by following the evolution of the complex moments of the fluid domain $\Omega(t)$ [12, 16]:

$$\iint_{\Omega(t)} z^m dx\ dy, \qquad z = x + iy,$$

for $m = 0, 1, 2, \ldots$. This idea has also been used to study flows driven by a multipole [4]. In this paper we employ this approach.

We first calculate the time derivative of the moments in the standard way. More precisely,

$$\frac{d}{dt}\left[\iint_{\Omega(t)} z^m dx\ dy\right] = \int_{\partial\Omega(t)} z^m V_n ds = \int_{\partial\Omega(t)} z^m \frac{\partial\phi}{\partial\vec{n}} ds \tag{6}$$

for nonnegative integer m, where we have used (4) in generating the last equality. Choosing a small circular disk $D(\epsilon)$ with radius ϵ and center at the origin, and applying Green's theorem to the region $\Omega(t)\backslash D$, we get

$$\begin{aligned}\int_{\partial\Omega(t)\cup\partial D} z^m \frac{\partial\phi}{\partial\vec{n}} ds &= \int_{\partial\Omega(t)\cup\partial D} \phi\frac{\partial z^m}{\partial\vec{n}} ds \\ &= \int_{\partial D} \phi\frac{\partial z^m}{\partial\vec{n}} ds + \int_{\partial\Omega(t)} \tau\kappa\frac{\partial z^m}{\partial\vec{n}} ds,\end{aligned}$$

where we have used (2) in the last equality. Exploiting (3) and letting $\epsilon \to 0$ yields

$$\int_{\partial\Omega(t)} z^m \frac{\partial\phi}{\partial\vec{n}} ds = \tau \int_{\partial\Omega(t)} \kappa \frac{\partial z^m}{\partial\vec{n}} ds + 2pM\pi\delta_{mp}, \qquad m = 0, 1, 2, \ldots.$$

Here $\delta_{mp} = 1$ for $m = p$ and vanishes otherwise. This together with (6) gives

$$\frac{d}{dt}\left[\iint_{\Omega(t)} z^m dx\ dy\right] = \tau \int_{\partial\Omega(t)} \kappa \frac{\partial z^m}{\partial\vec{n}} ds + 2pM\pi\delta_{mp}, \qquad m = 0, 1, 2, \ldots. \tag{7}$$

Conversely, we shall use a simple argument similar to that of [16] to show that if the moments satisfy (7), then the corresponding $\{\Omega(t)\}$ is a solution.

Indeed, if $\phi(x, y, t)$ denotes the solution to the Dirichlet problem (1), (2), and (3), the argument before (7) shows that

$$\int_{\partial\Omega(t)} z^m \frac{\partial\phi}{\partial\vec{n}} ds = \tau \int_{\partial\Omega(t)} \kappa \frac{\partial z^m}{\partial\vec{n}} ds + 2pM\pi\delta_{mp}, \qquad m = 0, 1, 2, \ldots.$$

This, combined with the assumption that

$$\begin{aligned}\int_{\partial\Omega(t)} z^m V_n ds &= \frac{d}{dt}\left[\iint_{\Omega(t)} z^m dx\ dy\right] \\ &= \tau \int_{\partial\Omega(t)} \kappa \frac{\partial z^m}{\partial\vec{n}} ds + 2pM\pi\delta_{mp}, \qquad m = 0, 1, 2, \ldots,\end{aligned}$$

gives

$$\int_{\partial\Omega(t)} z^m \left[\frac{\partial\phi}{\partial\vec{n}} - V_n\right] ds = 0, \qquad m = 0, 1, 2, \ldots.$$

Continuous function $[\frac{\partial\phi}{\partial\vec{n}} - V_n]$ can be uniformly approximated by harmonic polynomials on $\partial\Omega(t)$ as closely as possible; this thus implies $V_n = \frac{\partial\phi}{\partial\vec{n}}$ on $\partial\Omega(t)$. Therefore $\{\Omega(t)\}$ is a Hele–Shaw solution.

We have therefore established the following theorem.

THEOREM 1. *Suppose that $\{\Omega(t)\}$ is a smooth family of simply connected domains. $\{\Omega(t)\}$ is a solution of the initial value problem for the Hele–Shaw flow if and only if its complex moments satisfy* (7).

We observe from (7) that a Hele–Shaw flow driven by a multipole with surface tension has two physical quantities whose time evolution is simple. The first one is the area of the fluid domain, which, in view of (7) at $m = 0$, is independent of time t. The second quantity is the linear complex moment of the fluid domain. Introducing the tangent angle θ, we evaluate the right-hand side of (7) when $m = 1$ to get

$$\begin{aligned}\frac{d}{dt}\iint_{\Omega(t)} z dx\ dy &= -i\tau \oint_{\partial\Omega(t)} \kappa[x'(s) + iy'(s)] ds + 2pM\pi\delta_{1p} \\ &= i\tau \oint_{\partial\Omega(t)} \theta_s e^{i\theta} ds + 2pM\pi\delta_{1p} \\ &= 2pM\pi\delta_{1p},\end{aligned} \tag{8}$$

where in the last equality we have used $\kappa = -\theta_s$ and $z_s = e^{i\theta}$; here s is the arclength.

In the case of a dipole, i.e., $p = 1$, (8) says that the linear moment is linear in time t. Since the area of the fluid domain is independent of t, the center of mass of the fluid domain is also linear in t and thus moves towards infinity when t becomes large. Therefore either the Hele–Shaw solution develops finite time singularities or the boundary of the fluid domain extends to infinity as t goes to infinity.

THEOREM 2. *For a Hele–Shaw flow driven by a dipole with surface tension, the boundary of the fluid domain either develops finite time singularities or extends to infinity as t goes to infinity.*

Theorem 2 indicates that, even when surface tension is present, singularity formation is inevitable if the flow is driven by a dipole. However, Theorem 2 does not determine the mechanism of the breakdown. It could be caused by topological changes of the fluid domain, by the interface's reaching the multipole, or perhaps by some other means. In the next two sections, we shall use numerical studies to determine possible types of singularity formation.

In the case of $p \geq 2$, (8) shows that the linear moment is time-independent. The area of the fluid domain is independent of time, and therefore so is the center of mass.

THEOREM 3. *For a Hele–Shaw flow driven by a multipole of order $p \geq 2$ with surface tension, the center of mass of the fluid domain is time-independent.*

The main implication of Theorem 3 is that a Hele–Shaw flow driven by a multipole of order ≥ 2 cannot approach any stationary solutions of Entov, Etingof, and Kleinbock if the initial center of mass of the fluid domain is away from the multipole. This follows from the facts that the center is time-independent and that all the stationary solutions have their centers of mass at the multipole [4]. It is therefore likely that such a flow will form singularities sooner or later, either in a finite time or in infinite time. We will use numerical computations to check whether this is true.

Special solutions of (7) can be easily found in the case of $\tau = 0$. Integrating (7) with $\tau = 0$ gives

$$\iint_{\Omega(t)} z^m dxdy = \iint_{\Omega(0)} z^m dxdy + 2pM\pi t\delta_{mp}, \qquad m = 0, 1, 2, \ldots. \tag{9}$$

We consider a family of domains $\{\Omega(t)\}$ which are the images of the unit disk $|w| < 1$ under the conformal maps of the form

$$f(w) = a_1(t)w + a_2(t)w^2 + a_3(t)w^3. \tag{10}$$

For simplicity, we want the coefficients to be real; this implies that the interface should have upper/lower symmetry.

The moment integral of (9) can be written as a contour integral,

$$\iint_{\Omega} z^m dxdy = \frac{1}{2i} \oint_{\partial\Omega} z^m \bar{z} dz.$$

We then calculate the contour integral with the boundary $\partial\Omega(t)$ given by the conformal mapping (10). Equation (9) reduces to three algebraic equations:

$$a_1^2(t) + 2a_2^2(t) + 3a_3^2(t) = a_1^2(0) + 2a_2^2(0) + 3a_3^2(0), \tag{11}$$

$$a_1^2(t)a_2(t) + 3a_1(t)a_2(t)a_3(t) = a_1^2(0)a_2(0) + 3a_1(0)a_2(0)a_3(0) + 2pMt\delta_{1p}, \tag{12}$$

$$a_1^3(t)a_3(t) = a_1^3(0)a_3(0) + 2pMt\delta_{2p}. \tag{13}$$

As a special case of (10)–(13), we obtain solutions for the case in which the initial fluid domain is a disk centered at the multipole. Namely, the domain is given by the

conformal mapping

$$f(w) = a_1(t)w + a_{p+1}(t)w^{p+1} \tag{14}$$

whose coefficients are governed by

$$a_1^2(t) + (p+1)a_{p+1}^2(t) = a_1^2(0), \tag{15}$$

$$a_1^{p+1}(t)a_{p+1}(t) = 2pMt. \tag{16}$$

In the above calculations, $p = 1$ or 2. However, (14)–(16) also hold for $p \geq 3$. Indeed, (14)–(16) were first found by Entov, Etingof, and Kleinbock [4]. They also showed that a Hele–Shaw solution given by (14)–(16) develops p symmetric cusps in a finite time. This breaking time can also be easily calculated [4].

3. Numerical methods. The numerical method for solving this free boundary problem is based on a boundary integral formulation. We first parameterize the boundary $\partial\Omega$ as $(x(\lambda,t), y(\lambda,t))$ with time-independent $\lambda \in [0, 2\pi)$. Then the boundary condition (2) can be written in terms of a singular integral equation,

$$-\frac{\sigma(\lambda)}{2} + \mathrm{Re}\left\{\frac{1}{2\pi i} P.V. \int_0^{2\pi} \frac{\sigma(\lambda')}{z(\lambda) - z(\lambda')} z_{\lambda'} d\lambda'\right\} = \tau\kappa + M\mathrm{Re}\left\{\frac{1}{z^p(\lambda)}\right\}, \tag{17}$$

which is, in fact, a Fredholm equation of the second kind. "P.V." stands for the principal integral, and $\sigma(\lambda)$ is the dipole strength. Once $\sigma(\lambda)$ is known, the normal component V_n of (4) can be calculated through the following integral:

$$V_n = \mathrm{Im}\left\{\frac{z_\lambda}{2\pi i|z_\lambda|} P.V. \int_0^{2\pi} \frac{\sigma_\lambda(\lambda')}{z(\lambda) - z(\lambda')} d\lambda' + \frac{pM}{z^{p+1}(\lambda)} \frac{z_\lambda}{|z_\lambda|}\right\}. \tag{18}$$

After V_n is calculated, the motion of the interface is determined through

$$(x_t, y_t) = V_n\vec{n} + T\vec{s}, \tag{19}$$

with V_n given by (17) and (18), where $\vec{s}$ is the unit tangent vector and T is the tangential component of the interface velocity. Notice that the tangential component T affects only the parameterization of Lagrangian points and does not affect the actual motion of the interface.

In order to overcome the difficulties of the strong stability constraints on the time-step due to the presence of surface tensions, we adapt the method developed by Hou, Lowengrub, and Shelley [6] to compute the evolution of the interface.

Let θ denote the tangent angle to the interface; then (19) in the complex form becomes

$$\begin{aligned} \frac{\partial}{\partial t}|z_\lambda| &= T_\lambda + V_n\theta_\lambda, \\ \theta_t &= \frac{T\theta_\lambda - V_{n\lambda}}{|z_\lambda|}. \end{aligned} \tag{20}$$

In particular, T of (19) is chosen such that $|z_\lambda|$ is everywhere equal to its mean, that is,

$$|z_\lambda(\lambda,t)| = \frac{1}{2\pi}\int_0^{2\pi} |z_{\lambda'}(\lambda',t)| d\lambda' = \frac{1}{2\pi} L(t), \tag{21}$$

where $L(t)$ is the length of the interface. By differentiating (21) with respect to t and using (20) we find

$$T(\lambda,t)=\frac{\lambda}{2\pi}\int_0^{2\pi}\theta_{\lambda'}V_n d\lambda'-\int_0^{\lambda}\theta_\lambda V_n d\lambda'. \tag{22}$$

Consequently, the evolution of the interface is now given in terms of L and θ by

$$\begin{aligned} L_t &= \int_0^{2\pi}\theta_\lambda V_n d\lambda,\\ \theta_t &= \frac{2\pi}{L}(T\theta_\lambda - V_{n\lambda}). \end{aligned} \tag{23}$$

Since σ of (17) is dominated by $-2\tau\kappa$ [6], we substitute these into (23) to obtain

$$\theta_t=\tau\left(\frac{2\pi}{L}\right)^3\mathcal{H}(\theta_{\lambda\lambda\lambda})+A(\lambda,t), \tag{24}$$

where $A(\lambda,t)$ is the remaining term with lower-order derivatives. In Fourier space, (24) is of the form

$$\hat{\theta}_t(k)=-\tau\left(\frac{2\pi}{L}\right)^3|k|^3\hat{\theta}(k)+\hat{A}(k),$$

which is linear for the term with the highest derivative. This form is convenient for a semi-implicit temporal integration. A straightforward Crank–Nicholson discretization on the linear term and a leapfrog on the nonlinearity give

$$\frac{\hat{\theta}^{n+1}(k)-\hat{\theta}^{n-1}(k)}{2\Delta t}=-\frac{\tau|k|^3}{2}\left[\left(\frac{2\pi}{L^{n+1}}\right)^3\hat{\theta}^{n+1}(k)+\left(\frac{2\pi}{L^{n-1}}\right)^3\hat{\theta}^{n-1}(k)\right]+\hat{A}^n(k).$$

The arclength L^{n+1} is computed through an explicit time integrator: the second-order Adams–Bashforth method. Together we have an explicit expression for $\hat{\theta}^{n+1}(k)$.

A pseudospectral method is applied to the spatial discretization [1, 10]. The numerical derivatives and integrations are taken through the discrete fast Fourier transform [5]. The integrals of (17) and (18) are approximated by the spectrally accurate trapezoidal method [14]. The Fredholm integral equation (17) is solved by the iterative procedure of the GMRES algorithm [13].

4. Description of numerical studies. We have done numerical computations for three kinds of multipoles: $p=1$, 2, and 3. The strength of the multipole is normalized to be $M=1$, and the length scale is determined by choosing the area of the fluid blob to be π. The Hele–Shaw solutions for $\tau=0$ were plotted by solving the corresponding algebraic equations, and those for $\tau\neq 0$ were computed using the numerical method of section 3.

Figures 1–6 depict solutions whose initial interface is the unit circle centered at the dipole. Figure 1 depicts the solution for $\tau=0$ at different times, and $t_{critical}$ stands for the time when a cusp is formed; the solution is given by (14)–(16). As proved by the analysis, a cusp is formed at the interface [4]. Figure 2 displays the solution for $\tau=1$ at various times. The computation was performed starting with $N=513$ and $\triangle t=5\times10^{-5}$ and was refined to $N=4096$ and $\triangle t=5\times10^{-8}$. Here N

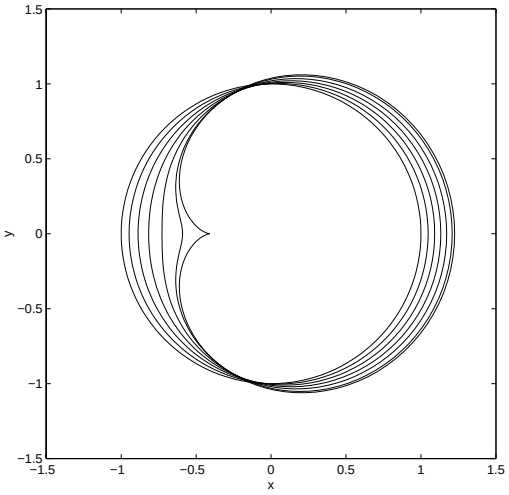

FIG. 1. *Time evolution of the initial circular interface for* $p = 1$ *with* $\tau = 0$ *at* $t = 0.025 \times i, i = 0, 5$*, and* $t = 0.136082$ *with* $0.136082 < t_{critical} < 0.136083$.

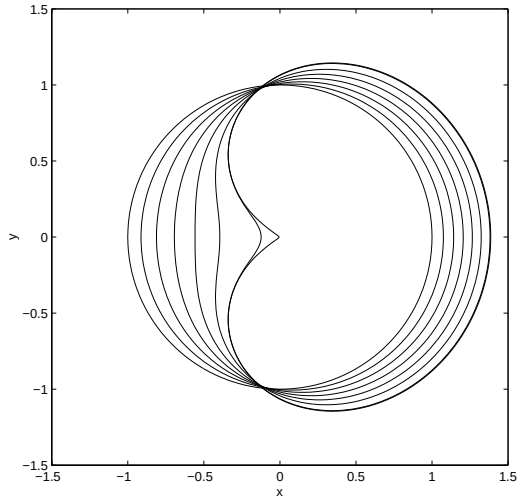

FIG. 2. *Time evolution of the initial circular interface for* $p = 1$ *with* $\tau = 1$ *at* $t = 0.04 \times (i - 1), i = 1, \ldots, 7$*, and final time* $t = 0.2427555$.

is the number of points used for spatial discretization. The behavior of the solution is rather similar to that of a sink flow [10]: The interface is seen to develop a finger that approaches the dipole as time evolves. As it touches the dipole, the finger appears to form a corner at its tip. The final time in our computation is $t = 0.24276$, which is far beyond the breaking time for $\tau = 0$.

The accuracy of the computations was studied by checking the resolution in the spatial variable and monitoring the evolution of the area and center of mass of the fluid blob. As mentioned in section 2, the area is time-independent, and the center moves in a constant velocity.

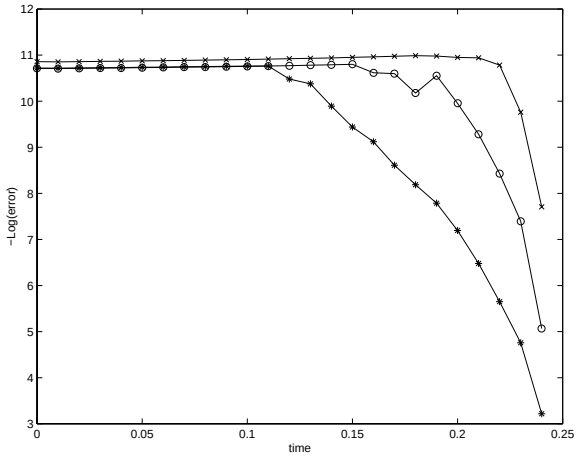

FIG. 3. *Spatial resolution study for $p = 1$ with $\tau = 1$. *: $N = 129$, o: $N = 256$, x: $N = 512$, and the highest resolution solution is computed using $N = 1024$. In all computations, $\triangle t = 5 \times 10^{-5}$.*

Figure 3 presents as a function of t the number of digits in the difference between computed solutions. The spatial convergence is demonstrated by comparing computations from $N = 129, 256$, or 512 with those from $N = 1024$. The errors are plotted on a negative logarithm vertical scale with a base 10. It is found that at earlier times the solution computed using $N = 512$ is accurate up to 10^{-11}, which is around the level of tolerance we specify for solving the integral equation (17). The accuracy deteriorates to about 10^{-8} when a finger is formed. The convergence of solutions is clearly demonstrated in Figure 3 as N increases.

We now estimate how fast the finger approaches the multipole. We will carry out our calculations for an arbitrary order p of the multipole. Since the finger is supposed to be very close to the multipole, in view of (3) we may assume that the velocity potential ϕ behaves like

$$\phi(x, y) = O\left(\frac{1}{r^p}\right) \qquad \text{as } r = \sqrt{x^2 + y^2} \to 0$$

in the neighborhood of the finger tip. We then use (4) to calculate the speed of the finger tip

$$V_n = O\left(\frac{1}{r^{p+1}}\right).$$

Denoting the distance between the finger tip and multipole at the origin by $D(t)$, we then have

$$\frac{dD(t)}{dt} = O\left(\frac{1}{[D(t)]^{p+1}}\right).$$

Integrating that equation yields

$$[D(t)]^{p+2} = O(t^* - t),$$

where t^* is the time at which the finger tip reaches the multipole. Consequently, we have

$$[D(t)]^{p+2} \approx C(t^* - t); \tag{25}$$

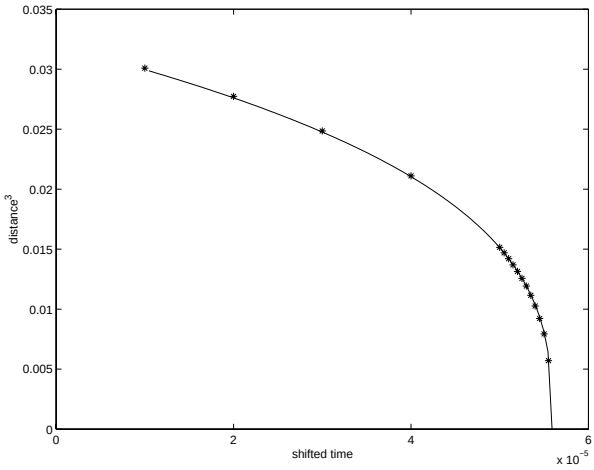

FIG. 4. *Distance between the finger tip and dipole with* $\tau = 1$. *Here time* $= 0.24270 +$ *shifted time; " * " represent the computed solutions, while the solid curve is the graph of* $[Distance]^3 = 0.39(0.2427559 - t)$.

here C is a time-independent constant.

We would like to mention that applying the above argument to Hele–Shaw flows driven by a sink will lead to a simple square root formula for the distance between the finger tip and sink. This parabolic behavior has been numerically confirmed in our previous paper [10].

Figure 4 shows the distance between the finger tip and dipole as a function of time. We can estimate $t^* = 0.2427559$ through extrapolation. By taking an average of the pointwise form-fit, we estimate $C = 0.39$ in (25) with $p = 1$. The solid curve is the graph of (25) as a function of a linearly shifted time. The "*" represent the distances obtained from the numerically computed solutions. The last computed solution is at $t = 0.2427555$. These two distances are seen to be in excellent agreement.

Figure 5 depicts the tangent angle θ as a function of λ around the tip at various times close to $t = 0.24276$. The interface is parameterized by a time-independent λ. The tangent angle displays a jump discontinuity at the tip when the finger touches the dipole. A linear extrapolation in time shows that the jump is about $\triangle\theta = 1.9$ radians. Hence the finger appears to form a corner at the tip with an acute angle $\pi - \triangle\theta$.

Figure 6 presents the solution whose initial data is exactly that of Figures 1 and 2; however, we now use a larger surface tension $\tau = 3$. The interface was computed by using $N = 512$ and $\triangle t = 10^{-4}$ at first, and by $N = 2048$ with $\triangle t = 10^{-5}$ at last. The distance between the last interface and dipole is about 0.028. For larger τ, the finger appears to be fatter and to approach the dipole at a slower pace. The finger also seems to form a corner with a larger angle at the tip.

Figures 7–9 show the solutions whose initial interface is given by (10) with $a_1(0) = \sqrt{11/12}$, $a_2(0) = 0$, and $a_3(0) = 1/6$. Figure 7 depicts the solution for $\tau = 0$. Two cusps are produced at the interface, and the breaking time is about $t_{critical} = 0.1601$. For $\tau = 0.02$, the two cusps are "regularized" by surface tension, and the interface forms two long fingers as shown in Figure 8. Eventually, the interface has the shape of a spade as the fingers reach the dipole. If larger τ is used, the interface dynamics are different. Figure 9 displays the solution for $\tau = 1$ at various times. Instead of two

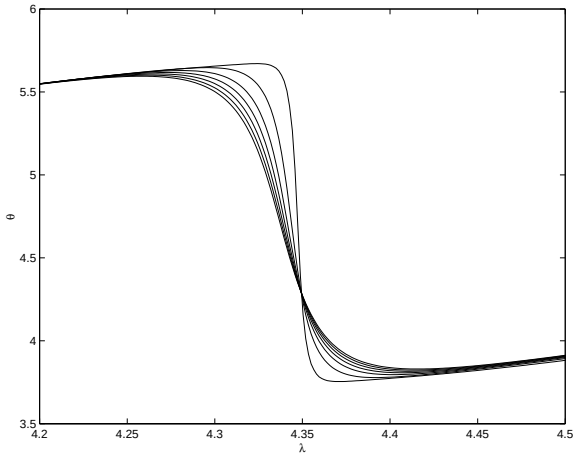

FIG. 5. *Tangent angle θ as a function of λ around the finger tip for $p = 1$ with $\tau = 1$ at $t = 0.2427 + 10^{-5} \times i, i = 0, \ldots, 5$, and final time $t = 0.2427555$.*

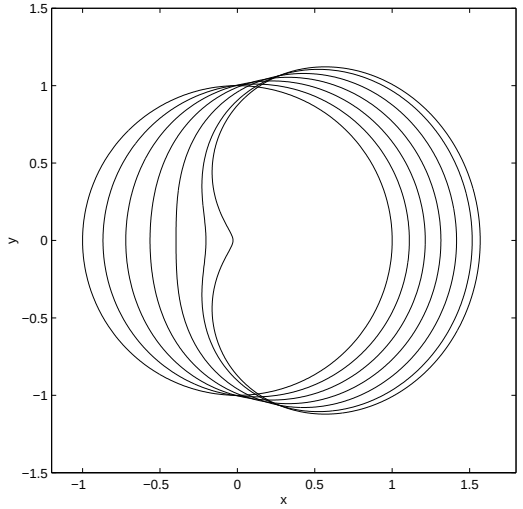

FIG. 6. *Time evolution of the initial circular interface for $p = 1$ with a larger surface tension $\tau = 3$ at $t = 0.06 \times (i - 1), i = 1, \ldots, 6$, and final time $t = 0.331$.*

fingers, one finger is developed and it reaches the sink at about $t = 0.2564$. For this case we also observe that the angle of the finger in Figure 9 is about the same as the one in Figure 2.

Why do the interfaces of Figures 2, 6, 8, and 9 always approach the dipole from the left? This can be explained by examining (5). Namely, that equation suggests that a dipole can be considered as a system with a source of strength $\frac{1}{2\epsilon}$ at $z = \epsilon$ and a sink of the same strength at $z = -\epsilon$ in the limit $\epsilon \to 0$. This amounts to putting a "source" to the immediate right of the origin and a "sink" to the immediate left. The "sink" will suck the fluid, causing the interface to reach the dipole from the left.

We now turn our attention to the case of $p = 2$. According to (5), a quadrupole

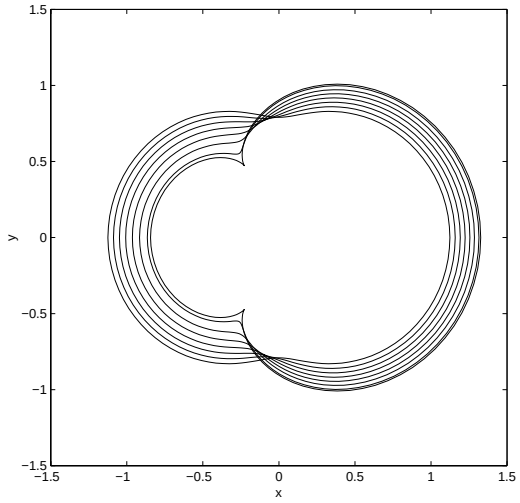

FIG. 7. *Time evolution of the "two cusps" initial interface for* $p = 1$ *with* $\tau = 0$ *at* $t = 0.0125 \times i, i = 0, 5$, *and* $t = 0.16005234$; $0.16005234 < t_{critical} < 0.16005235$.

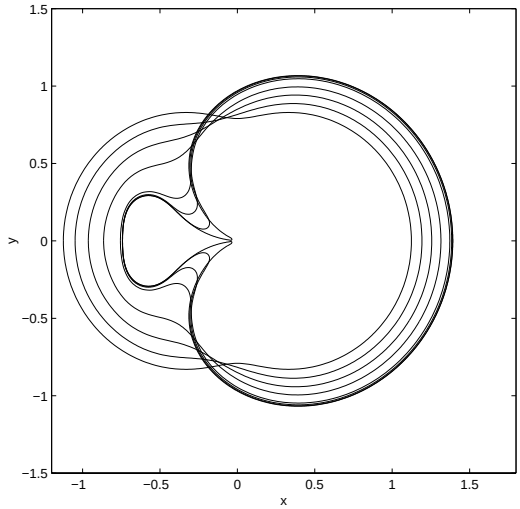

FIG. 8. *Time evolution of the "two cusps" initial interface for* $p = 1$ *with* $\tau = 0.02$ *at* $t = 0.05 \times i, i = 0, \ldots, 4$, *and* $t = 0.21, 0.215, 0.2165$.

at the origin is equivalent to a system of two sources and two sinks of large intensity. The sources are to the immediate left and right of the origin, and the sinks are just above and below the origin. Hence when it approaches the quadrupole the interface is expected to do so from above or below.

Figures 10–14 depict solutions whose initial interface is a unit circle centered at the quadrupole. Figures 10 and 11 display the solutions for $\tau = 0$ and $\tau = 1$, respectively. The $\tau = 0$ interface moves towards the quadrupole from the top and bottom, and eventually develops two cusps. These two cusps are regularized by the surface tension $\tau = 1$ in Figure 11. Instead, two fingers are formed to reach the quadrupole from

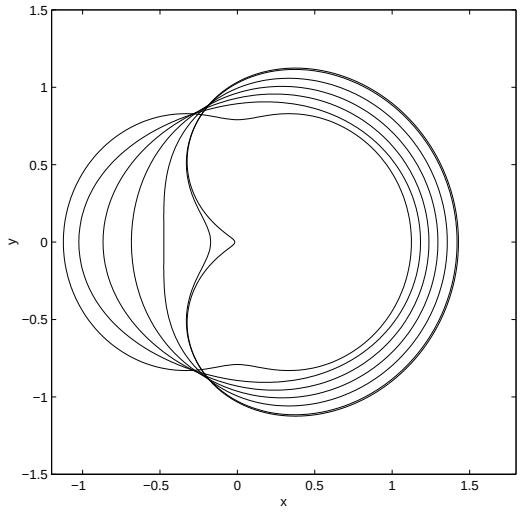

FIG. 9. *Time evolution of the "two cusps" initial interface for* $p = 1$ *with* $\tau = 1$ *at* $t = 0.05 \times i, i = 0, \ldots, 5$, *and* $t = 0.256425$.

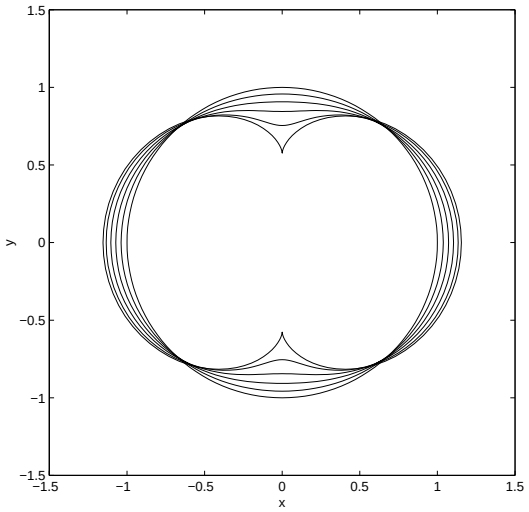

FIG. 10. *Time evolution of the initial circular interface for* $p = 2$ *with* $\tau = 0$ *at* $t = 0.01 \times i, i = 0, \ldots, 4$, *and* $t = 0.0468750$; $0.0468750 < t_{critical} < 0.0468751$.

both above and below the origin, as predicted by (5). The computation was started with $N = 512$ and $\triangle t = 5 \times 10^{-5}$ and then was refined up to $N = 4096$ with $\triangle t = 2 \times 10^{-8}$. The use of very small time-steps is essential in order to resolve the extremely fast motion of the interface when the two parts of the interfaces pinch.

Figure 12 shows the tangent angle as a function of the parameter λ around a finger tip at various times. Again we see a jump discontinuity in the tangent angle, and it is at about 2.8. Hence the finger forms a corner when it touches the quadrupole.

Figure 13 depicts the distances between the finger tip and quadrupole. The distances are obtained in two ways: One is from the direct numerical simulation and

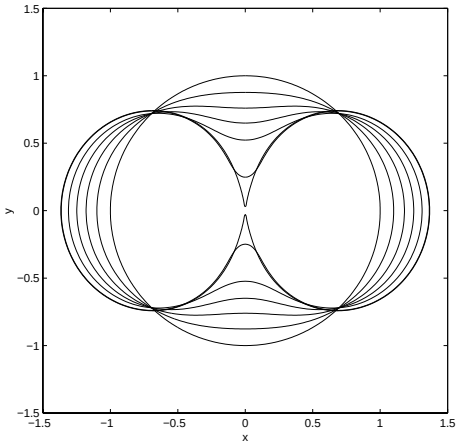

FIG. 11. *Time evolution of the initial circular interface for* $p = 2$ *with* $\tau = 1$ *at* $t = 0.03 \times i, i = 0, \ldots, 6$, *for* $t = 0.146$ *and* $t = 0.1468164$.

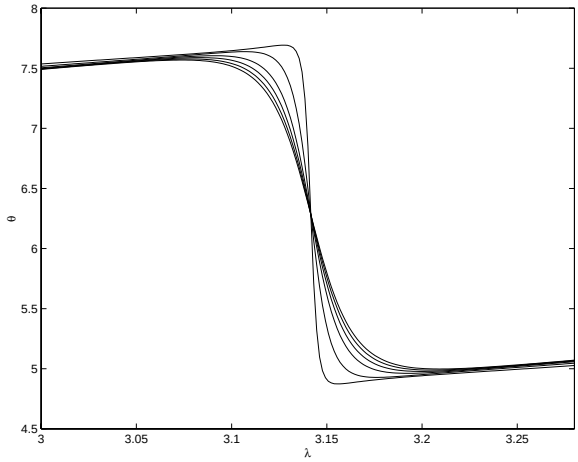

FIG. 12. *Tangent angle* θ *as a function of* λ *around a finger tip for* $p = 2$ *with* $\tau = 1$ *at* $t = 0.146795 + 5 \times 10^{-6} \times i, i = 0, \ldots,$ *and* $t = 0.1468164$.

the other from (25) with $p = 2$. We obtain $t^* = 0.07566766$ and $C = 12.72$ by an extrapolation and estimate similar to the case for $p = 1$. The agreement between the direct simulation and (25) seems to be very good.

Figure 14 represents the solution whose initial interface is exactly that of Figure 11; however, we now use a larger surface tension $\tau = 3$. The computation was performed using $N = 129$ and $\Delta t = 5 \times 10^{-5}$. The interface seems to approach a fixed interface as t increases. One expects this equilibrium interface to be a time-independent Hele–Shaw solution; indeed, this is the case. In Figure 14 we also display one of the stationary solutions found by Entov, Etingof, and Kleinbock [4]. The stationary solution matches the fixed interface very well. The convergence of the time-dependent solution to the stationary solution is shown in Figure 15. Figure 15(a) plots the distance between the time-dependent and time-independent interfaces

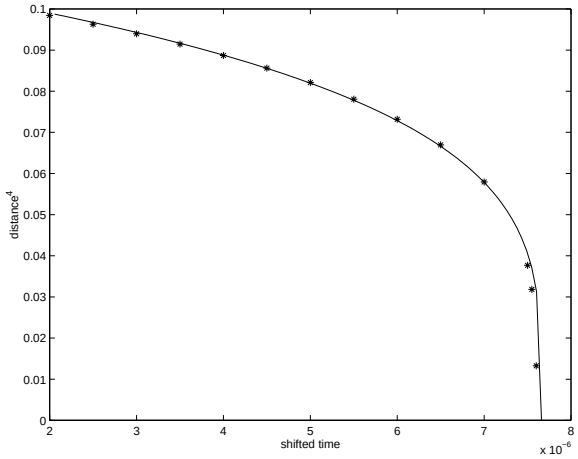

FIG. 13. *Distance between the finger tips and quadrupole for* $\tau = 1$. *Here time* $= 0.07566 +$ *shifted time; "*" indicates the computed solution; and the solid curve is the graph of* $[Distance]^4 = 12.72(0.07566766 - t)$.

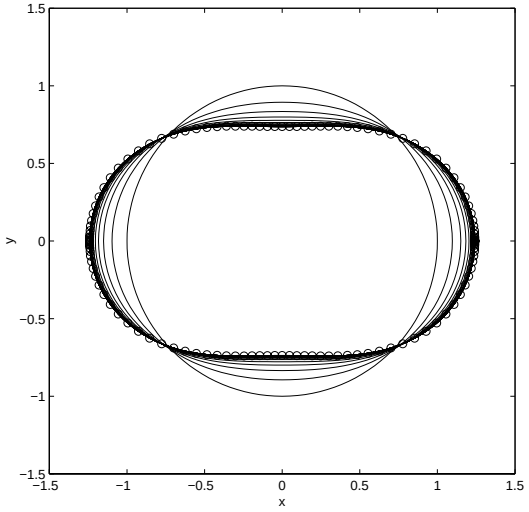

FIG. 14. *Large time evolution of the initial circular interface for* $p = 2$ *with a larger surface tension* $\tau = 3$. o*: the exact stationary solution; curves: time-dependent solutions at time* $= 0.1 \times i/3$, $i = 0, \ldots, 28$.

on a logarithmic vertical scale with base 10. The former interface is seen to approach the latter one exponentially fast. This is consistent with what Kelly and Hinch found in their numerical computations [9]. To check the accuracy of this large time computation, we monitor the evolution of the area and center of mass. Figure 15(b) displays the errors between the computed area and center and the exact ones. The latter are in theory independent of time. The errors are also plotted on a logarithmic vertical scale. The computation of the center is accurate to around 10^{-6}, and that of area to around 10^{-7}.

We now move the initial interface of Figure 14 a little bit so that its center is away from the quadrupole and then compute the solution for the same τ. Now singularity

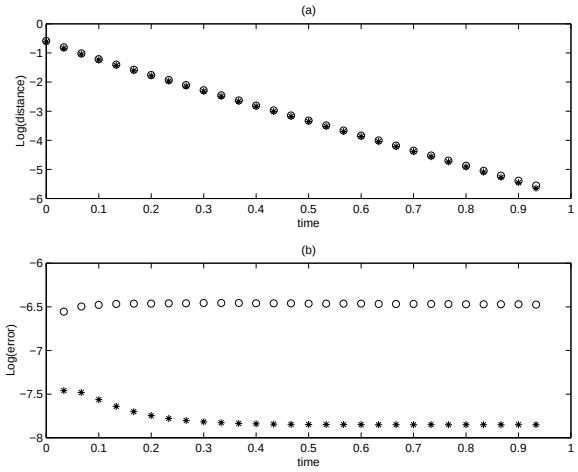

FIG. 15. *Error in large surface tension computations:* (a) *The distance between the stationary solution and time-dependent solution as a function of time . "*": at the intersection of the positive x-axis,* o*: at the intersection of positive y-axis.* (b) *The errors in conserved quantities as functions of time. "*": area,* o*: center.*

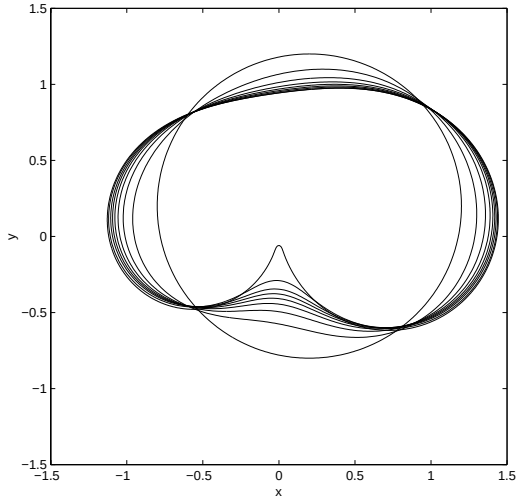

FIG. 16. *Time evolution of the initial circular interface centered at* $(0.2, 0.2)$ *for* $p = 2$ *with* $\tau = 3$ *at* $t = 0.05 \times i, i = 0, \ldots, 7$*, and* $t = 0.366745$.

formation is observed again. Figure 16 depicts the solution for $\tau = 3$ when the initial interface is a unit circle centered not at the origin but at $(0.2, 0.2)$. A finger is seen to reach the quadrupole from below.

Figures 17 and 18 depict the solutions whose initial interface is given by (10) with $a_1(0) = \sqrt{11/12}$, $a_2(0) = \sqrt{1/24}$, and $a_3(0) = 0$. Figure 17 displays the solutions at various times for $\tau = 0$, and Figure 18 for $\tau = 1$. When $\tau = 1$, two fingers are formed, and they move to the quadrupole from above and below. The behavior of the interface is very similar to that of Figure 10 even though their initial interfaces are quite different.

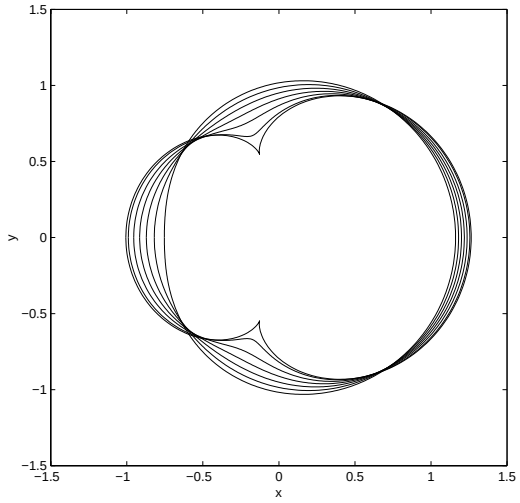

FIG. 17. *Time evolution of the "two cusps" initial interface for* $p = 2$ *with* $\tau = 0$ *at* $t = 0.008 \times i, i = 0, \ldots, 5$, *and* $t = 0.0438048$; $0.0438048 < t_{critical} < 0.0438049$.

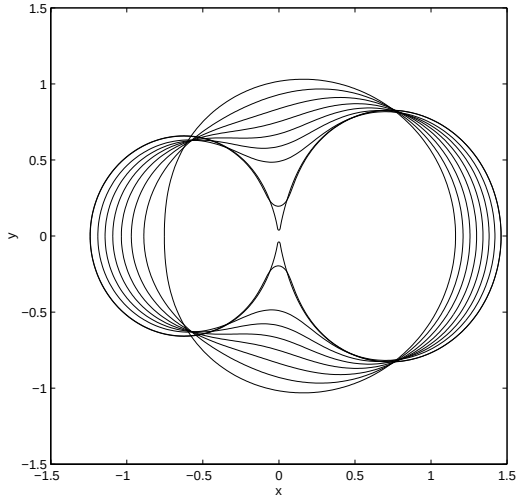

FIG. 18. *Time evolution of the "two cusps" initial interface for* $p = 2$ *with* $\tau = 1$ *at* $t = 0.02 \times i, i = 0, \ldots, 7$, *and* $t = 0.14025$.

Finally, we will present numerical results for the case of $p = 3$. Figure 19 shows the $\tau = 0$ solution whose initial interface is a circle centered at the multipole. The interface moves towards the multipole from the directions whose polar angles are $\frac{\pi}{3}$, π, and $\frac{5\pi}{3}$, and it eventually develops three cusps. Figure 20 depicts the solution with $\tau = 1$ for the same initial interface. Three symmetric fingers are formed, and they reach the multipole from the above three directions. As before, these directions are predicted by (5).

Figure 21 displays the tangent angle of the interface as a function of the parameter λ around a finger tip at various times. We clearly see a jump in the tangent angle when

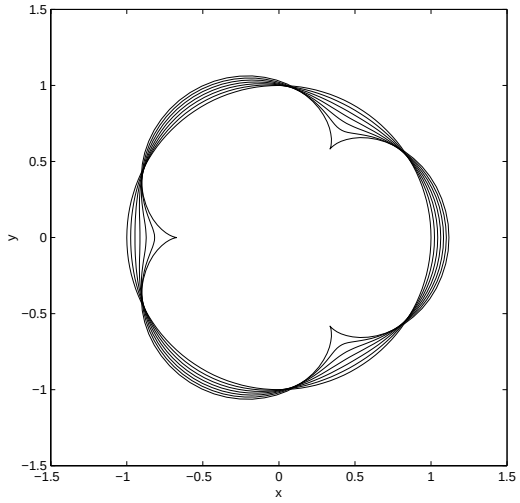

FIG. 19. *Time evolution of the initial circular interface for* $p = 3$ *with* $\tau = 0$ *at* $t = 0.004 \times i, i = 0, 5$, *and* $t = 0.0238513$; $0.0238513 < t_{critical} < 0.0238514$.

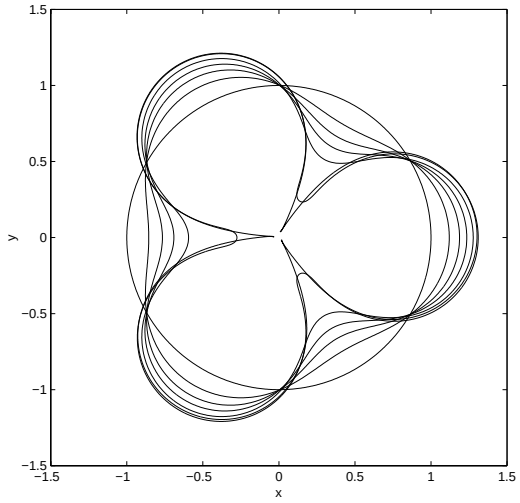

FIG. 20. *Time evolution of the initial circular interface for* $p = 3$ *with* $\tau = 1$ *at* $t = 0.03 \times (i - 1), i = 1, \ldots, 5$, $t = 0.1328$, *and* $t = 0.1329345$.

the finger touches the multipole. The jump is about 3.0 radians, and the resulting angle for the corner is as small as $\pi - 3.0$ radians. This angle is obviously smaller than its counterparts for $p = 1$ and 2 when other physical parameters, namely the intensity of the multipole and surface tension, are kept the same. This small angle explains why we observe a "cusp-like" shape at the tip of the finger when it touches the multipole, as shown in Figure 20.

Figure 22 depicts as a function of time the distance between the finger tip and multipole. Again we plot both the distances obtained from computed solutions and that obtained from (25) with $p = 3$. In this case, it is found that $t^* = 0.13829351$

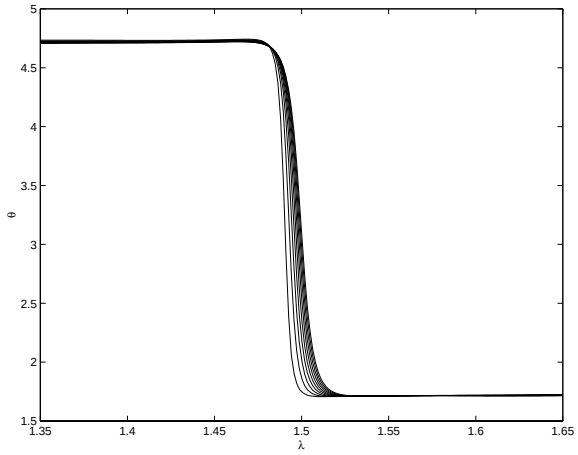

FIG. 21. *Tangent angle θ as a function of λ around a finger tip for $p = 3$ with $\tau = 1$ at $t = 0.13293 + 5 \times 10^{-7} \times i, i = 0, \ldots, 9$.*

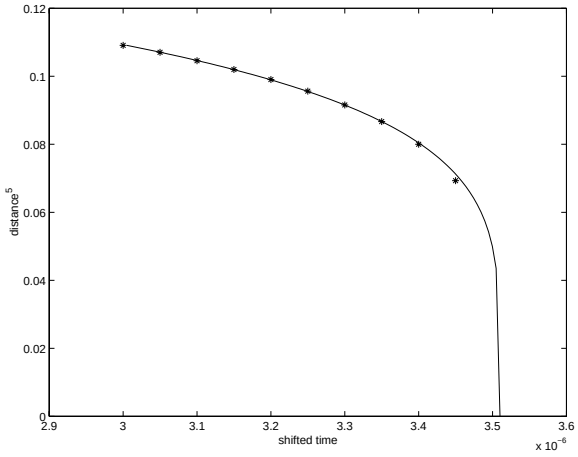

FIG. 22. *Distance between the finger tips and multipole for $p = 3$ with $\tau = 1$. Time = 0.13829 + shifted time, "*" represents the computed solution, while the solid curve is the graph of $[Distance]^5 = 24.48(0.13829351 - t)$.*

and $C = 2.04$ in (25). Since the interface accelerates to the multipole much faster than the cases for $p = 1$ and $p = 2$, and since the finger appears to be narrower, we cannot continue to compute the interface as close to the multipole as in the other cases. Nevertheless, the agreement between the direct numerical simulation and (25) is still very good up to the final time in our computed solutions.

We now increase the surface tension to $\tau = 3$ without changing the initial interface of Figure 20. The solution is seen to approach a stationary solution when time is large, as shown in Figure 23.

We then move the initial interface of Figure 23 so that the center is at the point $(-0.2, -0.2)$ and compute the solution for the same surface tension $\tau = 3$. Figure 24 depicts the resulting solution at various times. This time only one finger is developed, and it reaches the multipole from the direction whose polar angle is $\frac{\pi}{3}$.

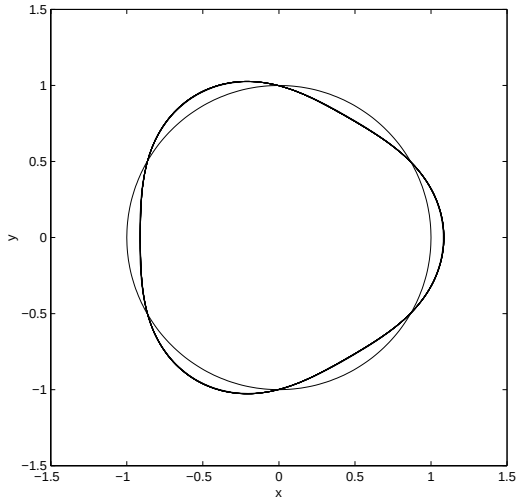

FIG. 23. *Large time evolution of the initial circular interface for* $p = 3$ *with a larger surface tension* $\tau = 3$ *at* $t = 0.05 \times i, i = 0, \ldots, 10$. *The final interfaces are not distinguishable from the stationary interface.*

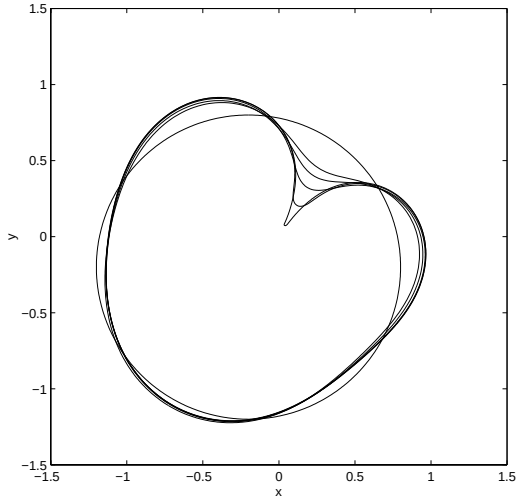

FIG. 24. *Time evolution of the initial circular interface centered at* $(-0.2, -0.2)$ *for* $p = 3$ *with* $\tau = 3$ *at* $t = 0, 0.05, 0.1, 0.128, 0.1308,$ *and* 0.13087.

From our numerical calculations, we observe that the size of the corner is independent of the initial shape of the interfaces, with all other parameters being the same. For example, for $p = 1$ and $\tau = 1$, three initial shapes have been studied: a circle with the center at the pole, a circle with the center not at the pole, and an initial shape as shown in Figure 9. It is found that the corner has a size of $\pi - \triangle\theta$, where $\triangle\theta = 1.9$ is accurate to two digits. Similar calculations are also performed for $p = 2, 3$, with $\tau = 1$, and the results are consistent with the case for $p = 1$. In particular, for $\tau = 1$ we obtain $\triangle\theta = 2.8$ for $p = 2$ and $\triangle\theta = 3.0$ for $p = 3$. Both of the estimates are

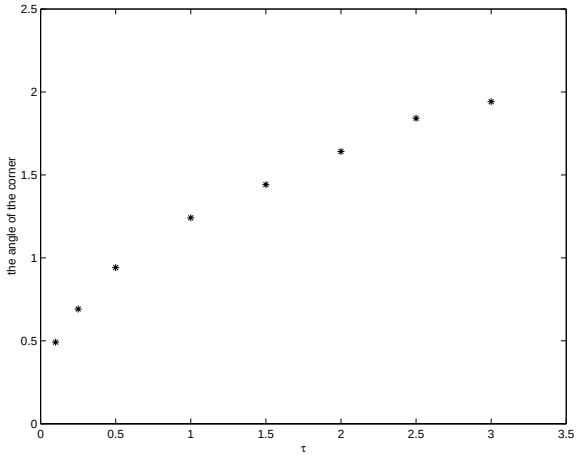

FIG. 25. *The angle of the corner as a function of the surface tension for* $p = 1$.

accurate to two digits. Moreover, for fixed p it is found that the size of the corner is an increasing function of τ. In Figure 25 we plot the angle of the corner as a function of τ for $p = 1$. How the angle depends on τ analytically is still an open problem.

Acknowledgments. The authors would like to thank J. Lowengrub and S. Tanveer for interesting discussions. The authors would also like to thank J. Hinch for his suggestions on the improvement of the manuscript.

REFERENCES

[1] G. R. Baker, D. I. Meiron, and S. A. Orszag, *Generalized vortex methods for free-surface flow problems,* J. Fluid Mech., 123 (1982), pp. 477–501.
[2] D. Bensimon, L. Kadanoff, S. Liang, B. Shraiman, and C. Tang, *Viscous flows in two dimensions,* Rev. Modern Phys., 58 (1986), pp. 977–999.
[3] H. Ceniceros, T. Hou, and H. Si, *Numerical study of Hele-Shaw flow with suction,* Phys. Fluids, 11 (1999), pp. 1042–1050.
[4] V. Entov, P. Etingof, and D. Kleinbock, *Hele-Shaw flows with a free boundary produced by multipoles,* European J. Appl. Math., 4 (1993), pp. 97–120.
[5] D. Gottlieb and S. A. Orszag, eds., *Numerical Analysis of Spectral Methods: Theory and Applications,* CBMS-NSF Regional Conf. Ser. Appl. Math. 26, SIAM, Philadelphia, PA, 1977.
[6] T. Y. Hou, J. S. Lowengrub, and M. J. Shelley, *Remove the stiffness from interfacial flows with surface tension,* J. Comput. Phys., 114 (1994), pp. 312–338.
[7] Y. E. Hohlov and S. D. Howison, *On the classification of solutions to the zero surface tension model for Hele-Shaw free boundary flows,* Quart. Appl. Math., 51 (1993), pp. 777–789.
[8] E. D. Kelley and E. J. Hinch, *Numerical simulations of sink flow in the Hele-Shaw cell with small surface tension,* European J. Appl. Math., 8 (1997), pp. 533–550.
[9] E. D. Kelley and E. J. Hinch, *Numerical simulations of Hele-Shaw flows driven by a quadrupole,* European J. Appl. Math., 8 (1997), pp. 551–566.
[10] Q. Nie and F. Tian, *Singularities in Hele-Shaw flows,* SIAM J. Appl. Math., 58 (1998), pp. 34–54.
[11] L. Paterson, *Radial fingering in a Hele-Shaw cell,* J. Fluid Mech., 113 (1981), pp. 513–529.
[12] S. Richardson, *Hele-Shaw flows with a free boundary produced by the injection of fluid into a narrow channel,* J. Fluid Mech., 56 (1972), pp. 609–618.
[13] Y. Saad and M. H. Schultz, *GMRES: A generalized minimal residual algorithm for nonsymmetric linear systems,* SIAM J. Sci. Comput., 7 (1986), pp. 856–869.
[14] A. Sidi and M. Israeli, *Quadrature methods for singular and weakly singular Fredholm integral equations,* J. Sci. Comput., 3 (1988), pp. 201–231.

[15] F. R. Tian, *On the breakdown of Hele-Shaw solutions with non-zero surface tension,* J. Nonlinear Sci., 5 (1995), pp. 479–484.
[16] F. R. Tian, *A Cauchy integral approach to Hele-Shaw problems with a free boundary: The case of zero surface tension,* Arch. Ration. Mech. Anal., 135 (1996), pp. 175–196.